forum acusticum 2026
8-12 September · Graz, Austria

A METAMATERIAL UNIT CELL DESIGN COMBINING MECHANICAL AND ACOUSTICAL RESONATORS FOR ENHANCED TRANSMISSION LOSS

Adam Cavanagh[1], Jordan Cheer[1]

[1] *Institute of Sound and Vibration Research, University of Southampton, UK*

Abstract

Locally resonant vibro-acoustic metamaterial panels have been shown to offer high sound transmission loss due to their stopband behaviour. Such treatments can significantly reduce the reradiation of sound energy in the stopband by reducing the panel's local vibration. However, the increased transmission loss occurs over a narrow frequency band and is usually followed by a pronounced reduction in the transmission loss, hindering the broadband performance. This work proposes a metamaterial unit cell concept that combines mechanical and acoustical resonators to mitigate the dip in the transmission loss and thus enhance the overall transmission loss over a targeted frequency range. A numerical model of the coupled configuration is developed to gain insights into the structural and acoustical dynamics, and their mutual interaction. A parametric study is performed to analyse the combined effects of the mechanical and acoustical resonator geometry on the transmission loss. Then, an optimisation procedure is implemented to obtain an optimal unit cell design for maximum attenuation. The numerical results indicate that the hybrid design can significantly reduce the minimum transmission loss while maintaining the stopband maximum, thus enhancing the broadband attenuation. The findings demonstrate that integrating mechanical and acoustical resonators within a unit cell offers a promising route toward compact, effective sound-insulating metamaterials.

Keywords: *Mechanical Resonator, Acoustical Resonator, Transmission Loss, Acoustic Metamaterial*

1. Introduction

Lightweight sound-insulating structures are important in applications where conventional mass-based treatments are impractical. Sound transmission loss generally increases with mass density for a uniform panel, as described by the classical mass law, see Eq. (2) [1]. Increasing mass is often unsuitable when compact, lightweight solutions are required. Locally resonant acoustic and vibroacoustic metamaterials offer an alternative means of modifying the dynamic response of a host structure using subwavelength resonators to achieve enhanced attenuation in a target frequency range [2], [3].

Vibroacoustic metamaterial panels usually use mechanical, mass-spring-type resonators embedded in or attached to a host panel. These resonators can move out of phase with the host structure near resonance, thereby reducing the local vibration and, hence, the reradiated sound power on the receiving side. This behaviour generates a pronounced stopband and an increase in the structure's transmission loss without significantly increasing the mass. However, the stopband is confined to a relatively narrow frequency range and is followed by a substantial reduction in transmission loss. This reduction is associated with the in-phase motion of the mass resonator; an asymmetric peak-dip resonance structure such as this is often interpreted as Fano-like interference [4]. This limits the treatment's broadband usefulness because a strong localised peak is less valuable when accompanied by a similarly strong dip.

Acoustic resonators offer an additional mechanism for controlling the response. Helmholtz resonators introduce an acoustic compliance–intertance resonance, whose frequency can be tuned by adjusting the neck and cavity dimensions [5]. Such resonators can strongly modify the effective acoustic impedance and produce enhanced attenuation around their resonance when introduced into acoustic metamaterials [6]. Coupled or multi-resonant designs have been investigated to broaden the useful bandwidth and mitigate the limitations of single-resonator systems [7].

This paper proposes a hybrid metamaterial unit cell

Corresponding author: *A.A.Cavanagh@soton.ac.uk.*

that combines a mechanical mass resonator and an acoustic Helmholtz resonator into a single unit cell. The mechanical resonator provides the main local-resonance stopband, whereas the Helmholtz resonator is tuned to reduce the severity of the post-stopband transmission-loss reduction. A three-dimensional finite-element model is developed to examine the coupled vibroacoustic response of the metamaterial under normal incidence. A parametric study is first used to investigate the influence of the Helmholtz resonator neck length, followed by a parametric optimisation to fine-tune the neck length and side lengths to minimise the reduction in transmission loss. The resulting combined design is compared with an equivalent-mass uniform panel, a mass-resonator-only configuration, and a Helmholtz-resonator-only configuration to assess whether the hybrid unit cell improves the metamaterial's broadband transmission-loss performance.

2. Metamaterial Description

The present metamaterial is based on a periodic unit cell embedded in a thin host panel. The unit cell combines two distinct substructures: a mechanical mass resonator (MR) and an acoustic Helmholtz resonator (HR). The purpose of this configuration is to exploit the stopband behaviour associated with the MR while reducing the pronounced transmission-loss dip immediately above this band. The MR is intended to reduce the panel's local vibration, thereby enhancing its transmission-loss performance, whereas the HR introduces an additional acoustic compliance-inertance resonance in the unit cell. By combining these mechanisms, the design provides an additional degree of freedom in controlling the transmission-loss response over a target frequency range.

2.1. Mass Resonator

The MR structure comprises a mass connected to the host structure by two thin legs that serve as compliant supports for the mass; see Fig. 1. This forms a mass-spring system similar to that in [8], whose resonance frequency is determined primarily by the resonator mass and the stiffness of the connecting legs. Near resonance, the attached mass exhibits out-of-phase motion relative to the host panel's vibration (anti-resonance), reducing the panel's overall vibration and thus the reradiation of sound energy on the receiving side.

The dimensions of the attached mass and its connected legs are the main design variables of the MR. Increasing the resonator mass or reducing the leg stiffness (by lowering their thickness) lowers the resonance frequency. Conversely, increasing the stiffness shifts the resonance frequency up. Thus, the MR structure offers a relatively simple means of tuning the stop band to a given frequency range. However, due to its asymmetric peak-dip resonance behaviour, the MR will exhibit a region near resonance in which its motion is in phase with the host structure, resulting in a pronounced reduction in transmission loss. This reduction may be addressed by introducing a second resonator with a monopolar resonance, such as a Helmholtz resonator.

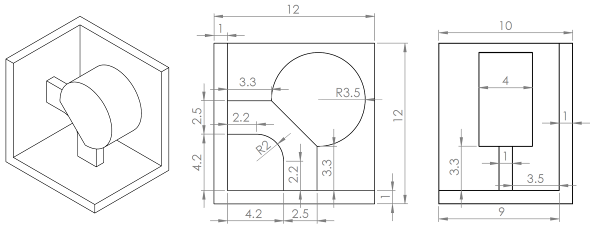

Figure 1: Dimensions of the mass resonator unit cell. All in millimetres.

2.2. Helmholtz Resonator

The acoustical component of the unit cell is a Helmholtz resonator, shown in Fig. 2 with the MR elements removed. Its cavity is formed by the outer walls of the unit cell, and the neck, positioned at one of its corners, extends into the unit cell. The air in the neck acts as an acoustic mass that oscillates against the compressible air in the cavity. The resonance frequency is controlled by the neck's cross-sectional area and length, the cavity volume, and any end corrections associated with the radiation discontinuity on both ends of the neck.

The HR provides a pressure-driven monopolar resonance in the unit cell. At and around its resonance frequency, the HR can strongly modify the acoustic impedance seen by a wave impinging on the panel structure. In the present design, this is used to counteract the dip in transmission loss occurring in the MR-only configuration. The HR geometry offers a second tuning mechanism separate from the MR's structural resonance. This allows tuning the unit cell's acoustic response according to the in-phase motion of the MR.

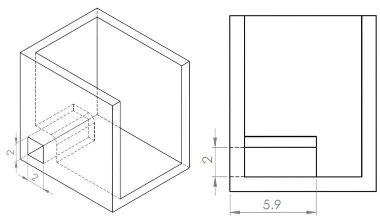

Figure 2: Dimensions of the Helmholtz resonator unit cell with some of the outer walls removed for clarity. All in millimetres. Note that only new dimensions are annotated; all others are as described in Fig. 2.

2.3. Combined Resonator Structure

The full metamaterial unit cell is obtained by combining the constituent MR and HR elements, as shown in Fig. 3. The mechanical and acoustical resonators become coupled elements of the same vibro-acoustic unit cell. An incident sound field excites both the panel's vibration and the oscillatory flow in the HR. The resulting transmission-loss response depends on the interaction between the MR's structural motion and the HR's acoustic impedance.

The combined unit cell is designed so that the MR maintains its anti-resonance stopband behaviour, while the HR mitigates the resonance transmission-loss dip that follows it. The design should exhibit improved broadband performance by tuning the HR in this way, which is important because a high but narrow transmission-loss peak loses practical value when accompanied by a severe reduction.

The geometry of the final unit cell is parameterised by the dimensions of its constituent resonators, with the MR and HR parameters controlling the structural and acoustic resonances, respectively. A parametric study is conducted on the HR neck length to evaluate its influence on the final transmission-loss response. The final HR dimensions (neck length and side lengths) to maximise sound attenuation are then obtained through a parameter optimisation procedure.

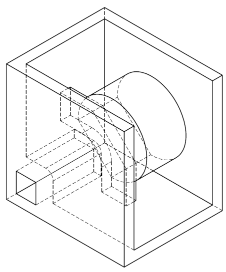

Figure 3: The combined resonator (mechanical and acoustical) unit cell. The dimensions of the constituent structures are shown in Fig. 1 and Fig. 2. Note that two of the outer wall segments are removed for clarity.

3. Numerical Model

3.1. Model Description

A three-dimensional numerical model is implemented in the commercial finite-element solver COMSOL Multiphysics® to understand the structural and acoustical dynamics of the metamaterial. The model consists of the unit cell sandwiched between two acoustic (fluid) domains representing the incident and transmitted sound fields, see Fig. 4. The structural and acoustic domains are modelled using the *Solid Mechanics* and frequency domain *Pressure Acoustics* interfaces. The *Acoustic-Structure* boundary condition is used to resolve the fluid load on the structure and thus its vibroacoustic behaviour.

Bloch-Floquet boundary conditions are applied to the opposing boundaries of the solid and fluid domains to simulate a metamaterial panel extending infinitely in the x- and y-planes. The wavenumbers are set to $k_x = k_y = 0$ rad/m, corresponding to normally incident excitation. The fluid properties are set to those of air using COMSOL's internal *air* material, i.e., with density $\rho_0 \approx 1.21$ kg/m^3 and sound speed $c_0 \approx 343$ m/s. Solid domains are modelled as a linear elastic material resembling typical Polylactic Acid (PLA) plastic with density $\rho = 1220$ kg/m^3, Young's modulus $E = 2.65$ GPa, Poisson's ratio $\nu = 0.35$, and damping implemented as an isotropic loss factor $\eta = 0.024$.

The model is acoustically excited and anechoically terminated using rectangular *Port* boundary conditions. The upper port in Fig. 4 excites the system with plane waves with pressure amplitude $p_0 = 1$ Pa, corresponding to a sound pressure level of approximately 94 dB. Only the plane-wave port mode is considered. The metamaterial's transmission loss TL (in dB) is calculated from the ratio of the incident to the transmitted sound power,

$$\mathrm{TL} = 10 \log_{10} \left(\frac{P_\mathrm{i}}{P_\mathrm{t}} \right) , \tag{1}$$

where P_i and P_t are the incident and transmitted sound powers, evaluated at the upper (inlet) and lower (outlet) ports, respectively. All simulations are solved over the frequency range 200–2000 Hz, in increments of 3–20 Hz, to achieve sufficiently fine frequency resolution in the structure's stop and passbands.

The additional damping arising from the losses in the viscothermal boundary layers in the HR neck is approximated with COMSOL's *Narrow Region Acoustics* formulation, which implements the equivalent fluid model described in [9]. The fluid properties are again defined by COMSOL's internal *air* material, with heat capacity at constant pressure $C_p \approx 1004.78$ J/(kg · K), specific heat ratio $\gamma = 1.4$, thermal conductivity $k \approx 0.026$ W/(m · K), bulk viscosity $\mu_B \approx 1.089\mathrm{e}-5$ Pa · s, and ρ_0 and c_0 as previously defined.

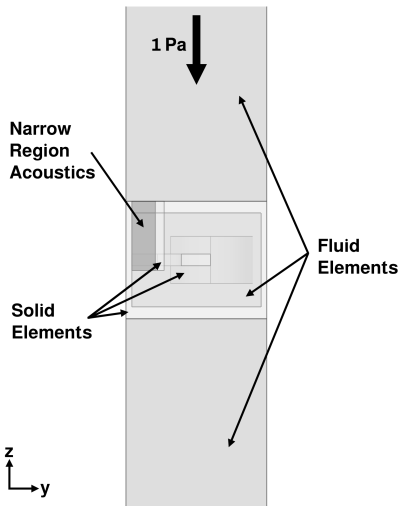

Figure 4: Illustration of the FEM model used to obtain the sound transmission loss of the metamaterial.

A coupled eigenfrequency study with Bloch-Floquet periodicity was also used to compute a dispersion diagram of the optimised unit cell along the Γ-X-M-Γ path. This path samples (with $N = 20$ equally spaced points) the standard high-symmetry directions of the square unit cell's Brillouin zone, from zero wavenumber (Γ) to the cell edge ($\mathrm{X} = \pi/L_x$), the zone corner ($\mathrm{M} = \pi/L_x + \pi/L_y$), and back to Γ [10], with the unit cell's x- and y-axis extents, or lengths $L_x = L_y = 12$ mm.

3.2. Meshing

The computational domains are discretised using quadratic tetrahedral elements, forming an unstructured mesh, as shown in Fig. 5. Periodic boundaries are imposed using identical meshes, meaning that the outer boundaries are mirror images of each other. The maximum element size in fluid domains is determined by the shortest acoustic wavelength in the sweep, such that six mesh elements per wavelength are produced, corresponding to the maximum element size of approximately 28.5 mm. Thanks to the use of the equivalent fluid model, the HR neck did not require a mesh sufficiently fine to resolve the viscous and thermal boundary layers.
The thinnest sections of the MR legs experience the greatest bending deformation when excited, resulting in higher stresses in these regions. Consequently, the edges in these regions are meshed with 35 mesh elements along their length to accurately resolve the stress gradients in the material. This refinement is visible in the right-hand panes of Fig. 5. The final mesh contained approximately 330,000 elements.

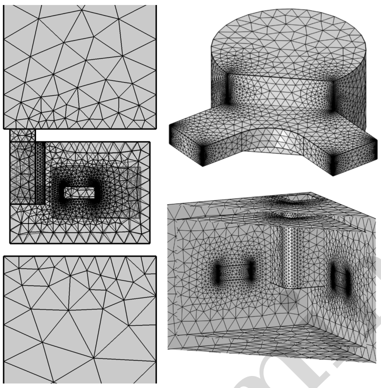

Figure 5: Illustration of the FEM model mesh. Left side: view of the fluid elements solving the Helmholtz equation. Right side upper: View of the solid elements forming the mass resonator. Right side lower: Section view of the solid elements forming the unit cell walls and Helmholtz resonator neck.

3.3. Validation Cases

Two additional models of the constituent resonators are implemented alongside the combined unit-cell model to understand their behaviour in isolation. The MR-only model has the same general setup but with the HR elements removed, as shown in Fig. 1. Likewise, the MR structure is removed in the HR-only model, as shown in Fig. 2. The incident and transmitted fluid domains are present in both models to obtain their transmission loss, as in the combined model. These models are implemented as described in Section 3.1, but with the appropriate elements removed.
The results from all three models are compared against a uniform panel with a mass close to that of the combined unit cell, the heaviest design considered. This panel's transmission loss $\mathrm{TL}_{\mathrm{ML}}$ (in dB) is given by the well-known mass law [1],

$$\mathrm{TL}_{\mathrm{ML}} = 20\,\log_{10}\left|1 + j\,\frac{2\pi f \rho d}{2\rho_0 c_0}\right|, \tag{2}$$

where $j = \sqrt{-1}$ is the imaginary unit, $d = 3.5\mathrm{e}{-3}$ m is the thickness of the panel giving a slightly larger mass than the combined unit cell, and f is frequency (in Hz). Eq. (2) gives the transmission loss of a uniform panel of infinite length and width and is thus appropriate to compare against the results with periodic boundary conditions shown hereinafter.

4. Parametric Study

A parametric study is conducted to investigate how the HR geometry affects the transmission-loss response of the combined unit cell. The HR neck length L_n is swept from 2 to 8.4 mm in 0.4 mm increments, while its side lengths and the geometry of the MR are fixed. The sweep is performed this way because neck length strongly affects the acoustic inertance of the HR, thereby providing a simple means of tuning its resonance frequency relative to the MR stopband.
The study described in Section 3.1 is solved to obtain the transmission loss of the unit cell at each L_n. The purpose of this study is to determine whether the HR can be tuned such that its added damping improves the minimum transmission loss in the frequency range immediately above the MR stopband, due to the in-phase motion of the MR and the host panel.

4.1. Results

The simulated transmission loss of the combined unit cell as a function of frequency and HR neck length L_n is shown in Fig. 6. As expected, the MR controls the metamaterial's main stopband, indicated by the high transmission loss associated with it remaining at approximately the same frequency, $f \approx 1200$ Hz, for all neck lengths. Increasing L_n increases the inertance of the fluid in the HR neck, shifting the HR transmission loss peak lower in frequency; see the second peak starting at $f \approx 1900$ Hz for $L_n = 2$ mm and approaching the $f \approx 1200$ Hz transmission loss maximum as $L_n \to 8.4$ mm.
The heatmap demonstrates that the HR can be tuned toward the post-stopband dip region. Shorter neck lengths place the HR effect at high frequencies, whereas longer necks shift it downward. In the present work, the most useful designs are those with $L_n \approx 6$ mm, where the post-stopband dip is reduced. This informs the subsequent optimisation procedure in Section 5.

5. Optimisation Procedure

A parameter optimisation was implemented following the parametric study to refine the HR geometry. The

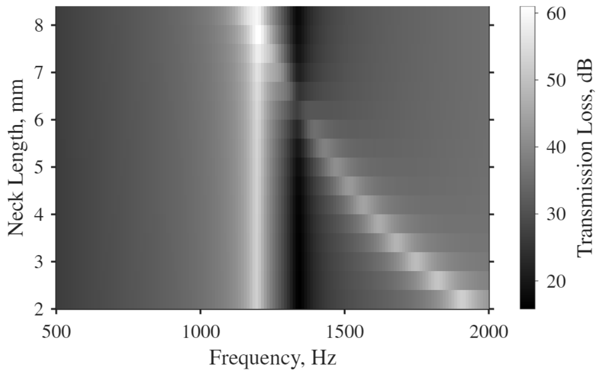

Figure 6: Heatmap showing the simulated transmission loss of the combined unit cell for neck lengths ranging from 2–8.4 mm in 0.4 mm increments.

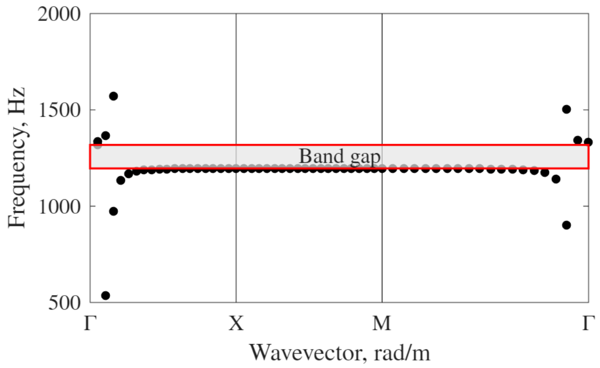

Figure 7: Dispersion diagram of the optimised coupled unit-cell model along the Γ-X-M-Γ path. The highlighted region indicates the structure's bandgap around 1200 Hz, where no propagating coupled vibroacoustic modes are predicted along the sampled directions.

MR geometry is again kept fixed so that the metamaterial's stopband does not change. The HR neck length L_n and neck side lengths a and b are used as the control variables to allow the solver to search for the neck geometry that best counteracts the post-stopband dip. The optimisation objective was to maximise the transmission loss across the frequency bands that cover the MR stopband and the higher-frequency dip. The objective function is evaluated over the discrete set

$$\mathbf{f} = [1150 : 12.5 : 1200] \cup [1300 : 12.5 : 1400] \text{ Hz} , \quad (3)$$

where the first and second sets cover the stopband and dip, respectively. The objective was

$$J(L_n, a, b) = \sum_{f \in \mathbf{f}} \mathrm{TL}(f; L_n, a, b) , \quad (4)$$

where $\mathrm{TL}(f; L_n, a, b)$ is the transmission loss of the combined unit cell with HR dimensions L_n, a, and b at each $f \in \mathbf{f}$. Maximising J favours HR geometries that improve the response across the stopband and dip regions, avoiding designs that might hinder the peak transmission loss. The variables were constrained to $0.5 \leq a, b \leq 3$ mm and $1 \leq L_n \leq 8.4$ mm.

6. Results

The optimised HR neck dimensions were $L_n = 5.9$ mm and $a = b = 2$ mm. Fig. 7 shows the coupled dispersion diagram of the optimised unit cell. A bandgap occurs at roughly 1200 Hz, aligning with the main transmission peak, shown in Fig. 8. This indicates that the peak is associated with the MR's local resonance stopband, where propagating coupled vibroacoustic modes are suppressed along the sampled directions.
The equivalent-mass panel follows the expected gradual increase in transmission loss with frequency, see Fig. 8. The MR-only response exhibits a strong stopband centred at $f = 1180$ Hz in the form of a pronounced transmission loss peak with a maximum value of 52.2 dB, almost 20 dB greater than the mass law at the same frequency. This corresponds to the MR's local resonance. As previously mentioned, however, this maximum is followed by a substantial reduction in transmission loss, which drops to 11.7 dB at 1375 Hz, nearly 24 dB below the mass-law curve.
The HR-only design exhibits a boost of up to 9 dB at and near its resonance frequency (1230 Hz) but is otherwise between 2.5 and 3.5 dB below the mass-law curve. This is expected because the mass-law curve is obtained for the full unit cell, which has a larger mass. The most important feature of the HR response is its monopolar resonance, which only increases attenuation rather than hindering it in the MR case.

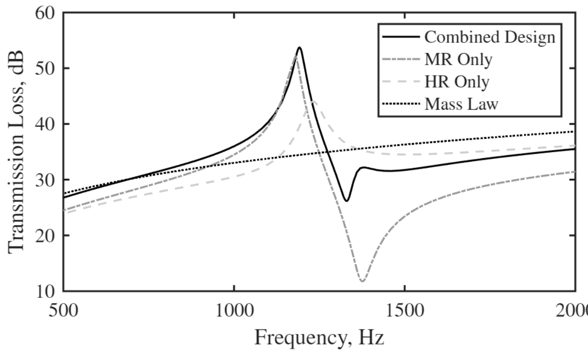

Figure 8: Simulated sound transmission loss of the different unit cell designs.

The combined unit cell with optimised HR dimensions exhibits the same general behaviour as the MR-only response up to its stopband, where the interactions between the two resonators become visible. The first notable feature is that the transmission-loss maximum increases to 53.7 dB at 1192 Hz, due to the overlap and cumulative effects of the HR and MR responses. Second, a pronounced minimum remains, but its effect on the high-frequency transmission-loss response is greatly reduced. Unlike the MR-only case, the combined unit cell follows the mass law closely below the main stopband. Again, this is expected since its mass is closest to that of the uniform reference panel.

Taken together, the dispersion and transmission-loss results show the complementary roles of the two resonators. The MR produces the main local-resonance stopband, as visible in Figs. 7 and 8. The HR modifies the acoustic response at frequencies above the main stopband, providing additional damping that mitigates the MR's post-stopband transmission-loss dip. The combined design therefore retains the useful high-transmission-loss peak while improving the metamaterial's broadband response.

7. Conclusions

A hybrid vibroacoustic metamaterial unit cell combining a mechanical mass resonator and an acoustic Helmholtz resonator was numerically investigated to enhance sound transmission loss. The coupled dispersion diagram showed a bandgap around 1200 Hz, associated with the main transmission loss peak. This confirms that the peak attenuation is attributed to the local-resonance stopband introduced by the mechanical resonator.

The mass-resonator-only design produced a strong stopband, but this was followed by a substantial post-stopband reduction in transmission loss. The parametric study showed that the Helmholtz resonator neck length provides an effective tuning parameter for controlling the acoustic response toward this dip region. The subsequent optimisation of the Helmholtz resonator neck dimensions produced a design that retained the main stopband peak while reducing the severity of the post-stopband attenuation.

These results show that the two resonators play complementary roles: the mechanical resonator suppresses the propagation of coupled vibroacoustic modes in the stopband, while the Helmholtz resonator improves the response above the stopband. This supports the use of coupled mechanical–acoustic resonator designs as a compact means for improved broadband sound-insulation performance.

8. Acknowledgments

This work was supported by the EPSRC and MOD Centre for Doctoral Training in Complex Integrated Systems for Defence and Security [EP/Y034848/1]. The authors acknowledge the use of the IRIDIS High Performance Computing Facility, and associated support services at the University of Southampton, in the completion of this work.

References

[1] F. Fahy and P. Gardonio, "Transmission of sound through partitions," in *Sound and Structural Vibration*, F. Fahy and P. Gardonio, Eds., 2nd Edition, Oxford: Academic Press, 2007, pp. 277–373, ISBN: 978-0-12-373633-8. DOI: 10.1016/B978-012373633-8/50009-0.

[2] Z. Liu et al., "Locally resonant sonic materials," *Science*, vol. 289, no. 5485, pp. 1734–1736, Sep. 2000, ISSN: 1095-9203. DOI: 10.1126/science.289.5485.1734.

[3] G. Ma and P. Sheng, "Acoustic metamaterials: From local resonances to broad horizons," *Science Advances*, vol. 2, no. 2, Feb. 2016, ISSN: 2375-2548. DOI: 10.1126/sciadv.1501595.

[4] C. Goffaux et al., "Evidence of fano-like interference phenomena in locally resonant materials," *Physical Review Letters*, vol. 88, no. 22, May 2002, ISSN: 1079-7114. DOI: 10.1103/physrevlett.88.225502.

[5] M. L. Munjal, *Acoustics of Ducts and Mufflers*, 2nd. Chichester, UK: John Wiley & Sons, 2014, ISBN: 978-1-118-44309-5.

[6] T. Yamamoto, "Acoustic metamaterial plate embedded with helmholtz resonators for extraordinary sound transmission loss," *Journal of Applied Physics*, vol. 123, no. 21, Jun. 2018, ISSN: 1089-7550. DOI: 10.1063/1.5025570.

[7] D. Roca and M. I. Hussein, "Broadband and intense sound transmission loss by a coupled-resonance acoustic metamaterial," *Physical Review Applied*, vol. 16, no. 5, Nov. 2021, ISSN: 2331-7019. DOI: 10.1103/physrevapplied.16.054018.

[8] C. Claeys, E. Deckers, B. Pluymers, and W. Desmet, "A lightweight vibro-acoustic metamaterial demonstrator: Numerical and experimental investigation," *Mechanical Systems and Signal Processing*, vol. 70-71, pp. 853–880, Mar. 2016, ISSN: 0888-3270. DOI: 10.1016/j.ymssp.2015.08.029.

[9] M. R. Stinson, "The propagation of plane sound waves in narrow and wide circular tubes, and generalization to uniform tubes of arbitrary cross-sectional shape," *The Journal of the Acoustical Society of America*, vol. 89, no. 2, pp. 550–558, Feb. 1991, ISSN: 1520-8524. DOI: 10.1121/1.400379.

[10] V. Cool, E. Deckers, L. Van Belle, and C. Claeys, "A guide to numerical dispersion curve calculations: Explanation, interpretation and basic matlab code," *Mechanical Systems and Signal Processing*, vol. 215, p. 111 393, Jun. 2024, ISSN: 0888-3270. DOI: 10.1016/j.ymssp.2024.111393.